Materials Today Energy 21 (2021) 100715

Contents lists available at ScienceDirect

Materials Today Energy

journal homepage: www.journals.elsevier.com/materials-today-energy/

Core–shell Co_3O_4@FeO_x catalysts for efficient oxygen evolution reaction

N. Liu , J. Guan *

Institute of Physical Chemistry, College of Chemistry, Jilin University, Changchun 130012, PR China

ARTICLE INFO

Article history:
Received 19 January 2021
Received in revised form
3 March 2021
Accepted 8 March 2021
Available online 13 March 2021

Keywords:
Cobalt oxide
Iron oxide
Graphite
Water oxidation
Water splitting

ABSTRACT

Rational fabrication of oxygen evolution reaction (OER) electrocatalysts based on earth-abundant elements is crucial for sustainable energy applications. Although Fe–Co-based (oxy)hydroxides show excellent catalytic activity for OER, a comprehensive understanding of the role of Fe and Co is still lacking. Here, we prepared a core–shell Co_3O_4@FeO_x catalyst with an ultrathin FeO_x (<1 nm) coating onto ultrafine Co_3O_4 nanoparticles (~3.1 nm), which exhibit higher OER activity than Fe/Co-based mixed oxides. The enhanced OER electrocatalytic performance is attributed to the introduction of ultrathin FeO_x, which can (1) combine water molecules to promote the reaction, (2) enhance the charge transfer ability of Co_3O_4, and (3) speed up the diffusion of the reactant water close to the active sites and the produced oxygen away from the active sites.

1. Introduction

To relieve environmental pollution from the consumption of fossil fuels, it is a doable way to convert intermittent energy (e.g. solar energy, hydroenergy, and wind energy) to electric energy and then to clean chemical energy (i.e. hydrogen) by electrolysis of water [1,2]. The electrochemical oxygen evolution reaction (OER) is the primary anode reaction for water splitting. The development of more efficient electrolyzers has been hindered by the lack of abundant, cost-effective, and stable alternatives to the state-of-the-art catalyst, iridium oxide [3]. Thus, the development of low-cost, efficient, and durable OER electrocatalysts becomes an unavoidable tendency [4].

In recent years, cobalt-based nanomaterials have been testified as one of the most promising non-precious metal electrocatalysts due to their high activity for the OER [5]. Various Co-based nanocomposites such as nitrides [6], phosphides [7], sulfides [8], selenides [9,10], oxides [11], and hydroxides [12] show OER activity in alkaline media. However, although these compounds can catalyze OER, most of them would transform partially or completely into (oxy)hydroxides under rigorous oxidizing conditions [9,13]. Therefore, Co-based mixed oxides have gained much attention for the OER in the last few years, especially for Fe–Co-based oxides [14–21]. Yeo et al. suggested that the improved OER activity of cobalt oxide should be related to the Fe sites with oxygen vacancies [14]. Zhu and co-workers also proposed that the improvement of OER activity over iron–cobalt oxide nanosheets might be attributed to oxygen vacancies, which could enhance electronic conductivity and accelerate the adsorption of water onto adjacent cobalt sites [22]. However, Boettcher et al. hold different views on the active site of $Co_{1-x}Fe_x(OOH)$ for the OER [23]. They hypothesized that the efficient active site should be the iron, while CoOOH only acts as a conductive parasitifer. Although there are some different views on the active site of Fe–Co-based (oxy)hydroxides, the synergistic effect between Fe and Co is generally accepted for the improved OER activity [24].

Generally, most Fe–Co-based (oxy)hydroxides were synthesized by mixing Fe- and Co-based precursors, which results in difficulty in identifying efficient active sites for the OER [25]. To better understand the role of Fe/Co in the OER, it is necessary to spatially separate them [26]. For instance, Hu et al. found that the OER performance of a single-atom catalyst Co–N–C-900 can be improved in a Fe^{3+}-containing KOH solution, and they proposed a dimeric Co–Fe moiety as the active center [24]. For oxides, different metal components can be segregated by core–shell nanostructures [27]. Herein, we fabricated a core–shell catalyst Co_3O_4@FeO_x with synergistic interactions between FeO_x nanoshells and Co_3O_4 nanoparticles, which shows higher OER activity than the uniformly dispersed $FeCoO_x$ catalyst.

* Corresponding author.
E-mail address: guanjq@jlu.edu.cn (J. Guan).

https://doi.org/10.1016/j.mtener.2021.100715
2468-6069/

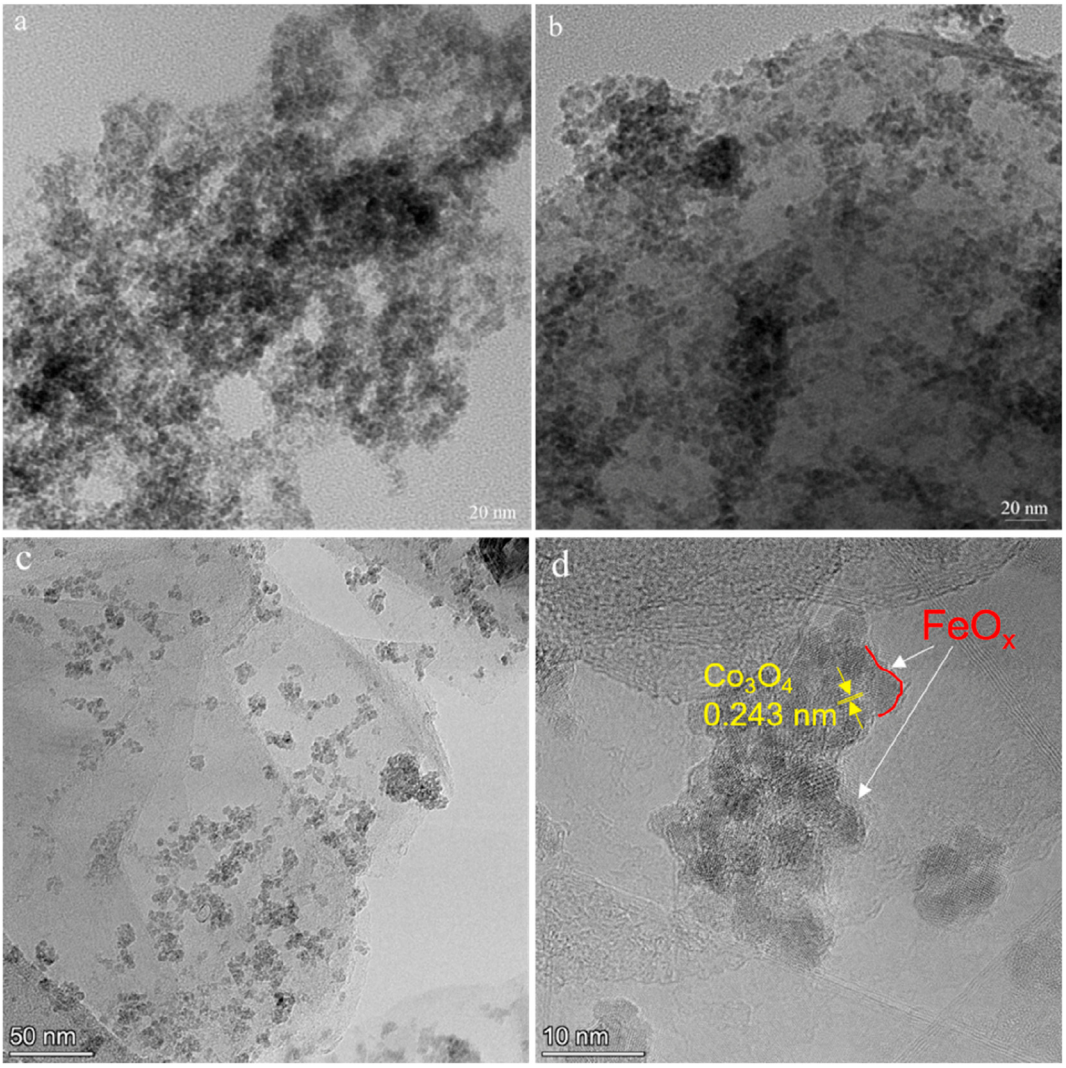

Fig. 1. (a) TEM image of Co_3O_4@FeO_x, (b) TEM image of 10%Co_3O_4@2%FeO_x/G-110, and (c–d) HRTEM images of 10%Co_3O_4@2%FeO_x/G-110.

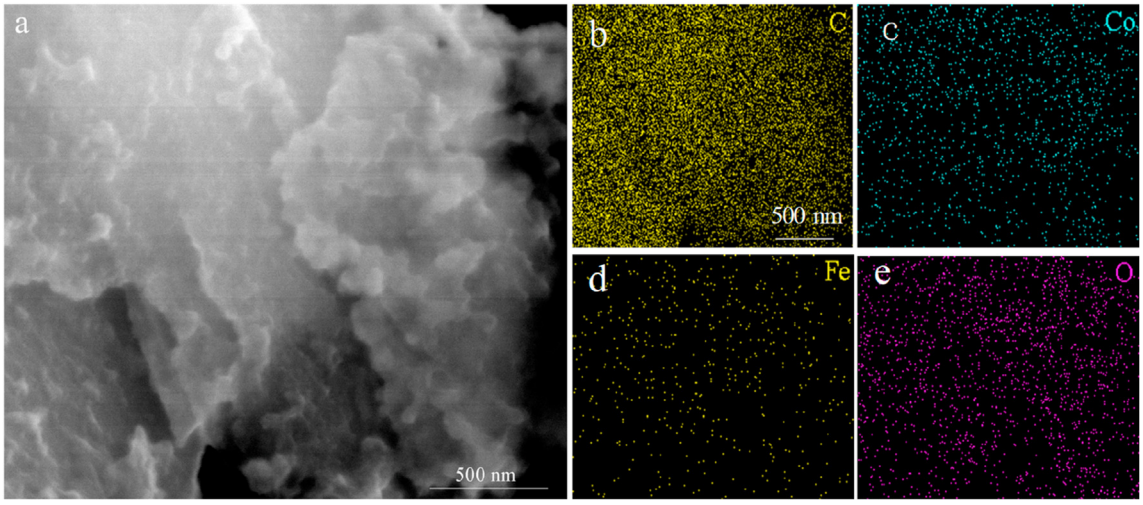

Fig. 2. (a) SEM image of 10%Co_3O_4@2%FeO_x/G-110 and (b–e) the corresponding EDS mapping of C, Co, Fe, and O.

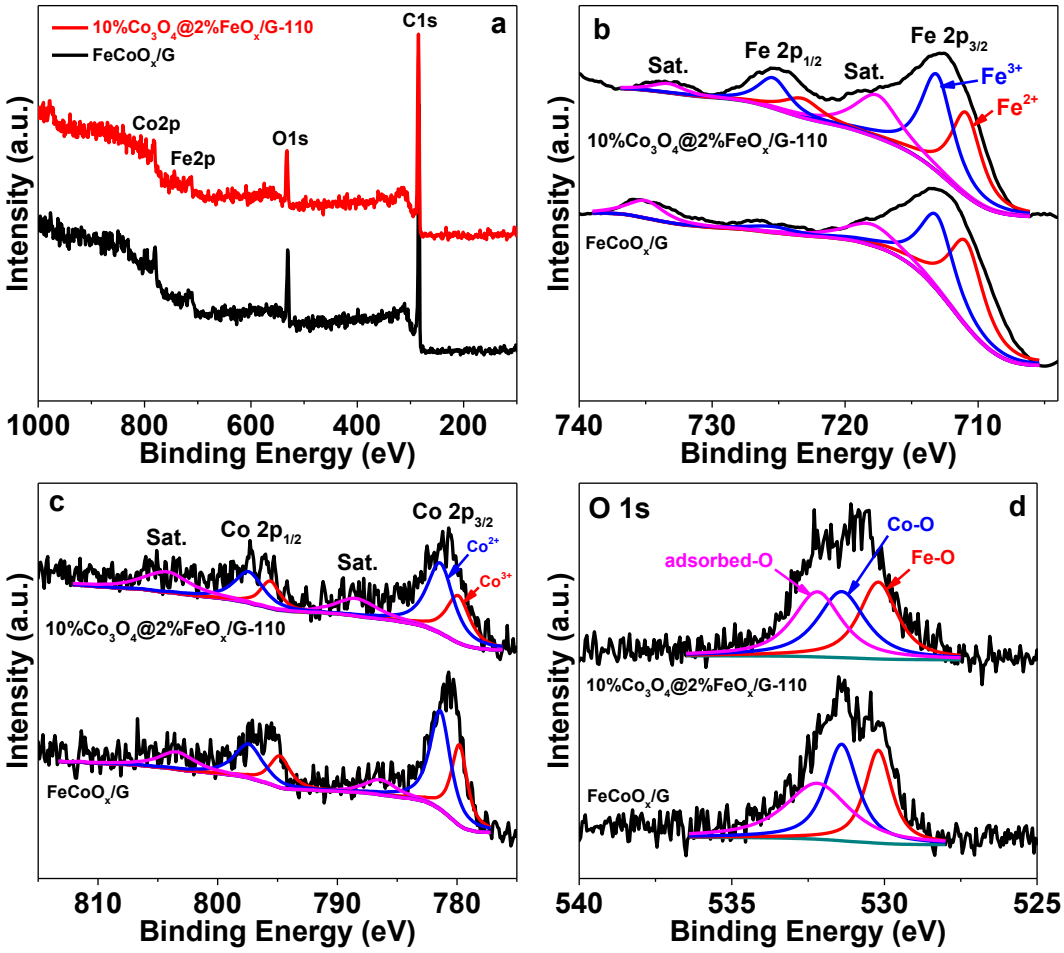

Fig. 3. (a) XPS survey spectra, (b) Fe 2p XPS spectra, (c) Co 2p XPS spectra, and (d) O 1s XPS spectra for $FeCoO_x$/G and 10%Co_3O_4@2%FeO_x/G-110.

2. Experimental section

2.1. Synthesis of Co_3O_4/G

To improve the hydrophilicity, graphite was treated with 20% oleum at 90 °C for 2 h. After filtering and washing, it was dried at 80 °C for 12 h. A certain amount of $CoCl_2 \cdot 6H_2O$, 0.1 g of oleum-treated graphite, and 50 μL of deionized water were dispersed in 20.0 mL of ethanol solution. Under stirring, 75 μL of 28% ammonia was added to the mixture. Afterward, it was transferred into a 30 mL Teflon autoclave and heated at 150 °C for 2 h. After cooling down, the solid was obtained by filtering, washing with water for several times, and drying at 80 °C overnight, which was denoted as Co_3O_4/G (where the percentage composition of Co is 5%, 10%, and 15%).

2.2. Synthesis of 10%Co_3O_4@n%FeO_x/G-110

A certain amount of $FeCl_3 \cdot 6H_2O$, 0.1 g of $Co_{10}O_x$@G, and 50 μL of deionized water were dispersed in 20.0 mL of ethanol solution. Under stirring, 25 μL of 28% ammonia was added to the mixture. Afterward, it was transferred into a 30 mL Teflon autoclave and heated at 110 °C for 2 h. After cooling down, the solid was obtained by filtering, washing with water for several times, and drying at 80 °C overnight, which was denoted as 10%Co_3O_4@n%FeO_x/G-110 (where n% represents the percentage composition of Fe, i.e. 1%, 2%, 3%, 4%, and 5%). The Co and Fe content in the 10%Co_3O_4@2%FeO_x/G-110 sample measured by ICP-AES is ca. 8.5 wt% and 1.8 wt%, respectively.

2.3. Synthesis of 10%Co_3O_4@2%FeO_x/G-T

In 20.0 mL of ethanol solution, 9.6 mg of $FeCl_3 \cdot 6H_2O$, 0.1 g of $Co_{10}O_x$@G, and 50 μL of deionized water were dispersed. Under stirring, 25 μL of 28% ammonia was added to the mixture. Afterward, it was transferred into a 30 mL Teflon autoclave and heated at different temperatures for 2 h. After cooling down, the solid was obtained by filtering, washing with water for several times, and drying at 80 °C overnight, which was denoted as 10%Co_3O_4@2% FeO_x/G-T (where T represents the crystallizing temperature, i.e. 100 °C, 110 °C, 120 °C, 130 °C, 140 °C, and 150 °C).

2.4. Synthesis of $FeCoO_x$/G

In 20.0 mL of ethanol solution, 9.6 mg of $FeCl_3 \cdot 6H_2O$, 40 mg of $CoCl_2 \cdot 6H_2O$, 0.1 g of oleum-treated graphite, and 50 μL of deionized water were dispersed. Under stirring, 25 μL of 28% ammonia was added to the mixture. Afterward, it was transferred into a 30 mL Teflon autoclave and heated at 150 °C for 2 h. After cooling down, the solid was obtained by filtering, washing with water for several times, and drying at 80 °C overnight, which was denoted as $FeCoO_x$/G.

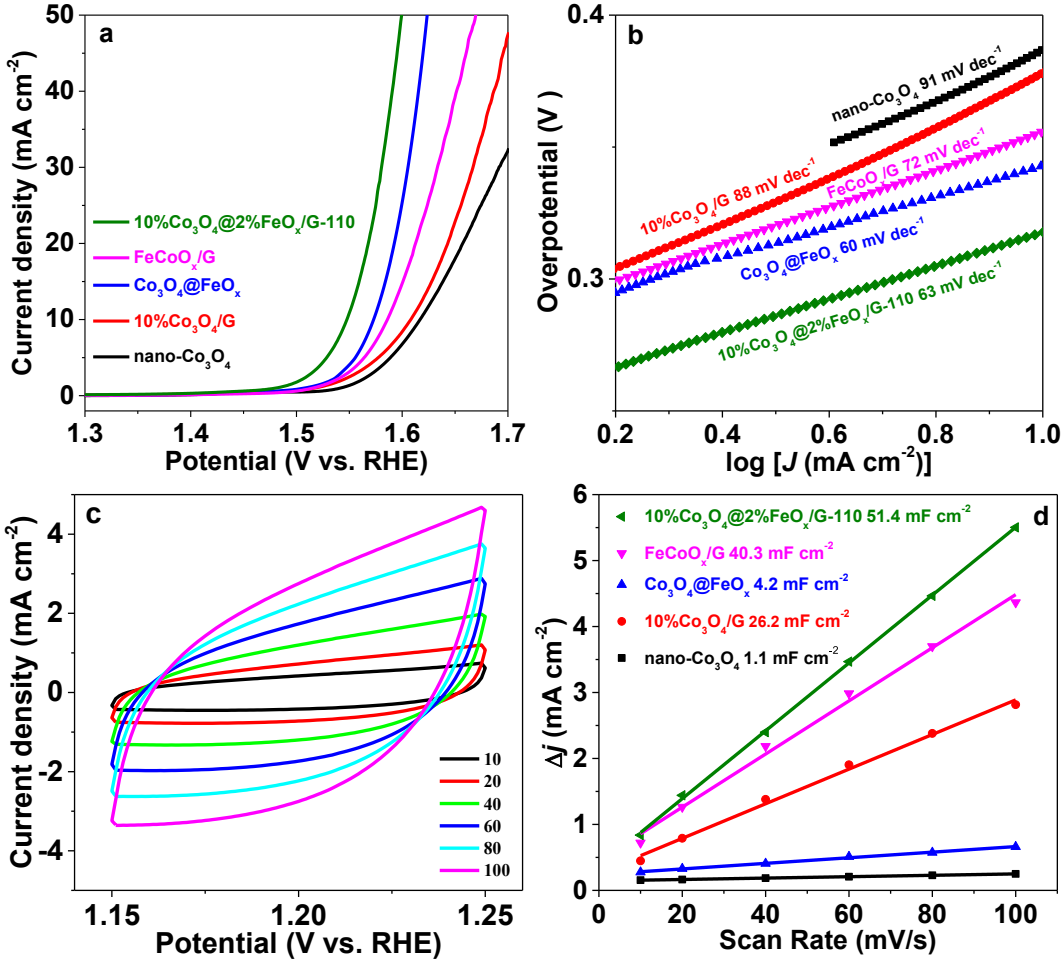

Fig. 4. (a) Polarization curves and (b) Tafel plots of the as-prepared samples. (c) CV curves of 10%Co_3O_4@2%FeO_x/G-110 and (d) Capacitive j vs scan rate.

2.5. Synthesis of nano-Co_3O_4 and Co_3O_4@FeO_x

To 20.0 mL of ethanol solution, 0.4 g of $CoCl_2 \cdot 6H_2O$ and 50 μL of deionized water were added. Under stirring, 750 μL of 28% ammonia was added to the mixture. Afterward, it was transferred into a 30 mL Teflon autoclave and heated at 150 °C for 2 h. After cooling down, the solid was obtained by filtering, washing with water for several times, and drying at 80 °C overnight, which was denoted as nano-Co_3O_4.

In 20.0 mL of ethanol solution, 96 mg of $FeCl_3 \cdot 6H_2O$, 400 mg of nano-Co_3O_4, and 50 μL of deionized water were dispersed. Under stirring, 25 μL of 28% ammonia was added to the mixture. Afterward, it was transferred into a 30 mL Teflon autoclave and heated at 110 °C for 2 h. After cooling down, the solid was obtained by filtering, washing with water for several times, and drying at 80 °C overnight, which was denoted as Co_3O_4@FeO_x.

3. Results and discussion

The morphology of the as-prepared samples was analyzed by TEM. As shown in Fig. 1a, ultrafine Co_3O_4@FeO_x nanoparticles with a size of less than 5 nm can be observed. After introducing an oleum-treated graphite support, the Co_3O_4@FeO_x nanoparticles were well dispersed (Fig. 1b). The species of the Co_3O_4@FeO_x nanoparticles on oleum-treated graphite was identified by HRTEM. As revealed in Fig. 1c and d, the Co species is in the form of Co_3O_4 with an average particle size of 3.1 nm, while the Fe species should be amorphous oxide or (oxy)hydroxide. For simplification, we labeled it as FeO_x. The dispersion of Fe/Co species was further analyzed by SEM-EDS. As shown in Fig. 2, the Fe/Co species are well distributed on the modified graphite.

The elemental compositions and chemical states of $FeCoO_x$/G and 10%Co_3O_4@2%FeO_x/G-110 were investigated by X-ray photoelectron spectroscopy (XPS). The XPS survey spectra show that the samples consist of C, O, Co, and Fe elements (Fig. 3a). In the high-resolution Fe 2p spectra, the Fe $2p_{3/2}$ peak can be convoluted into two peaks at 710.9 eV and 713.1 eV, ascribed to Fe^{2+} and Fe^{3+}, respectively (Fig. 3b) [28–31]. From Fig. 3c, the fitted Co $2p_{3/2}$ peak shows two main signals at the binding energies of 779.8 eV and 781.4 eV, attributed to Co^{3+} and Co^{2+}, respectively [32,33]. From Fig. 3d, the O 1s XPS spectra can be deconvoluted into three peaks, centered at 530.2 eV, 531.4 eV, and 532.2 eV, which are due to Fe–O, Co–O, and absorbed O, respectively [34,35]. The surface Fe/Co ratio in 10%Co_3O_4@2%FeO_x/G-110 is 0.62, much higher than that in $FeCoO_x$/G (0.38), implying different forms of dispersion of Fe in the two samples.

The electrocatalytic OER performance of 10%Co_3O_4@2%FeO_x/G-110 was evaluated by LSV in 1 M KOH. By contrast, nano-Co_3O_4, 10% Co_3O_4/G, Co_3O_4@FeO_x, and $FeCoO_x$/G were also investigated. As shown in Fig. 4a, the 10%Co_3O_4@2%FeO_x/G-110 demonstrates excellent OER activity with an overpotential (η_{10}) of 318 mV at 10 mA cm^{-2}, which is lower than those for nano-Co_3O_4 (388 mV),

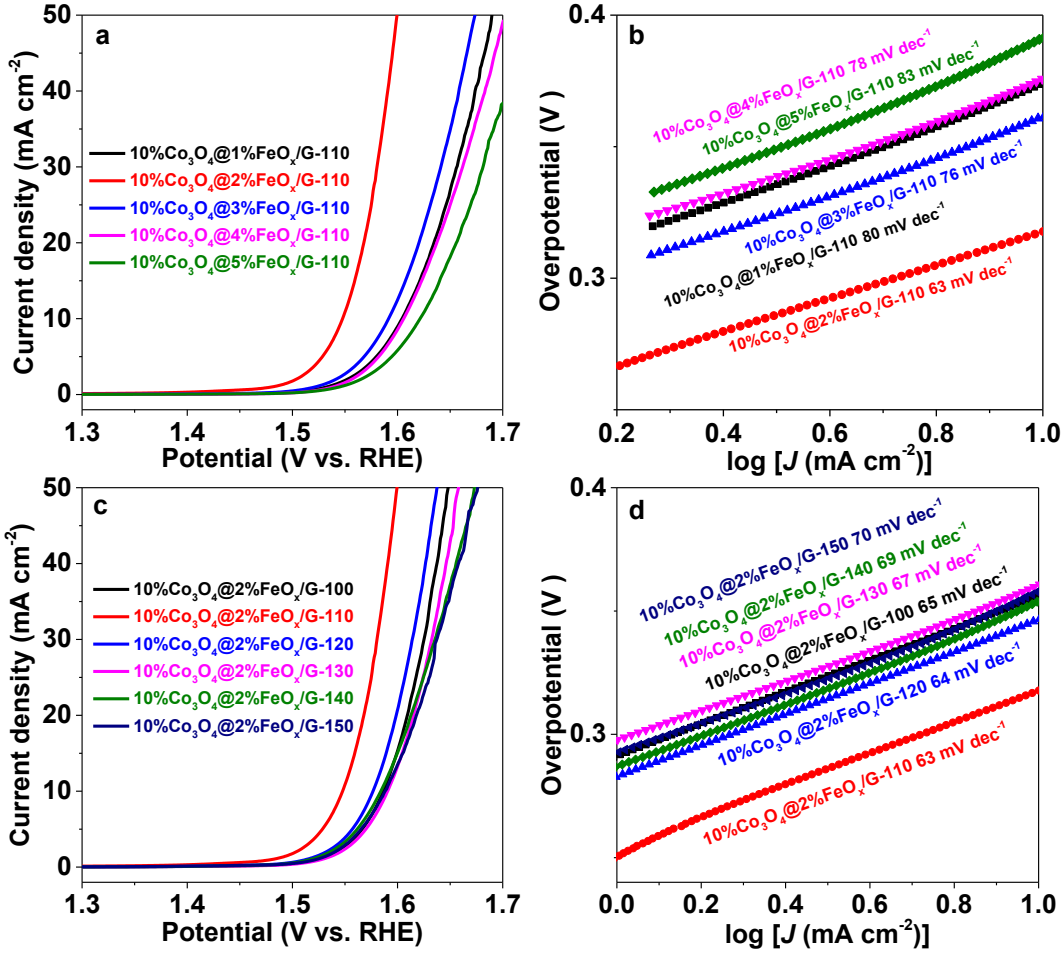

Fig. 5. (a) Polarization curves and (b) Tafel plots of 10%Co_3O_4@n%FeO_x/G-110. (c) Polarization curves and (d) Tafel plots of 10%Co_3O_4@2%FeO_x/G-T.

10%Co_3O_4/G (379 mV), Co_3O_4@FeO_x (344 mV), and $FeCoO_x$/G (357 mV) and most previously reported OER electrocatalysts (Table S1), such as ultrathin layered double CoFe hydroxide nanosheets (CoFe LDH, η_{10} = 331 mV) [36], NiFeOOH (η_{10} = 340 mV) [37], nickel–cobalt layered double hydroxides (Ni–Co LDHs, η_{10} = 350 mV) [38], and ultrathin cobalt–manganese layered double hydroxide (CoMn LDH, η_{10} = 324 mV) [39]. The corresponding Tafel slope of 10%Co_3O_4@2%FeO_x/G-110 is determined to be 63 mV decade^{-1}, which is much lower than 91 mV decade^{-1} for nano-Co_3O_4, 88 mV decade^{-1} for 10%Co_3O_4/G, and 72 mV decade^{-1} for $FeCoO_x$/G, demonstrating an accelerated OER kinetics on the 10%Co_3O_4@2%FeO_x/G-110 (Fig. 4b). Moreover, these results reveal that the location of the Fe element plays a key role in facilitating OER catalytic activity. When the cobalt and iron

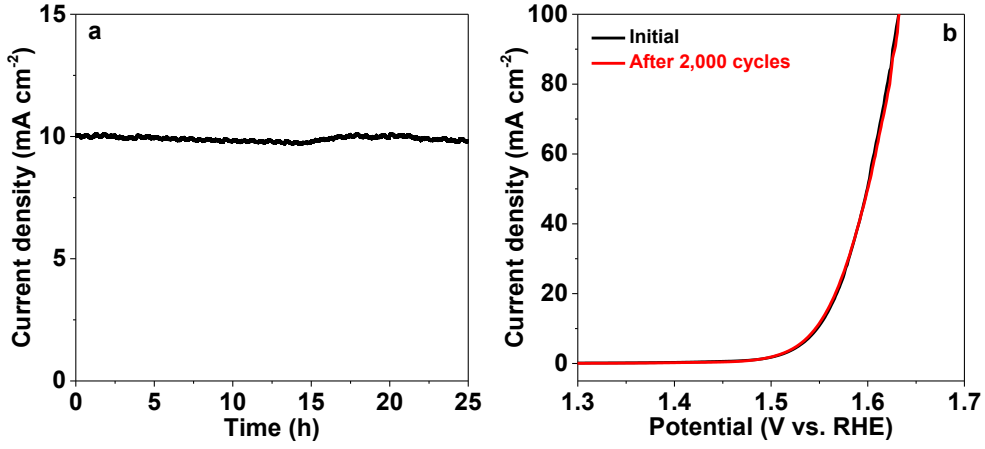

Fig. 6. (a) *I*–t curve and (b) polarization curves of 10%Co_3O_4@2%FeO_x/G-110 before and after CVs for 2000 cycles.

were coprecipitated onto the graphite ($FeCoO_x$/G), it shows higher OER activity than the Fe-free sample (10%Co_3O_4/G), indicating that both Fe and Co might take part in the OER process in agreement with previous reports [24,28]. However, Fe doping on the outer surface of cobalt oxide shows higher OER activity than that inside the cobalt oxide. For instance, the 10%Co_3O_4@2%FeO_x/G-110 shows much higher OER activity than $FeCoO_x$/G.

To further explore the role of Fe in the improvement of OER activity of Co_3O_4, the electrochemical surface area (ECSA) was measured. As illustrated in Fig. 4c and d, the linear slope for nano-Co_3O_4, 10%Co_3O_4/G, Co_3O_4@FeO_x, $FeCoO_x$/G, and 10%Co_3O_4@2%FeO_x/G-110 is 1.1, 26.2, 4.2, 40.3, and 51.4 mF cm^{-2}, respectively. It can be found that the linear slope of catalysts with Fe doping is larger than that without Fe doping, suggesting that more active sites are generated by Fe doping. Moreover, the core−shell catalyst 10%Co_3O_4@2%FeO_x/G-110 shows a larger slope than the Fe/Co-mixed catalyst $FeCoO_x$/G, indicating that the former could offer more active sites than the latter for the OER.

The synergistic action between Fe and Co for the OER was investigated by electrochemical impedance spectroscopy. As demonstrated in Fig. S1, it can be observed that there is an obvious semicircle in the high-frequencies for the nano-Co_3O_4, which is due to charge transfer resistance (Rct). After supporting FeO_x on the Co_3O_4, the semicircle becomes much smaller, indicating that the charge transfer ability is immensely improved. In addition, the straight line at the low-frequency region becomes steeper by doping Fe onto Co_3O_4, suggesting that the diffusion resistance becomes smaller, which favors the absorption of water onto the anode interface and diffusion of oxygen away from the active sites. The 10%Co_3O_4@2%FeO_x/G-110 catalyst shows better diffusion ability than nano-Co_3O_4, 10%Co_3O_4/G, Co_3O_4@FeO_x, and $FeCoO_x$/G, implying its superior electrochemical properties in agreement with the aforementioned OER results.

Since Fe plays a favorable role in promoting OER activity of Co_3O_4, its doping content was investigated. First, we investigated the optimal loading amount of Co_3O4 on the graphite for the OER. As depicted in Fig. S2, the 10%Co_3O_4/G shows higher OER activity than 5%Co_3O_4/G and 15%Co_3O_4/G, suggesting that moderate cobalt oxide loadings (i.e. 10 wt% Co loading) are conducive to the dispersion on the graphite support. Next, we studied the influence of Fe loading content on the OER performance. As shown in Fig. 5a, within the present experimental conditions, the 10%Co_3O_4@2%FeO_x/G-110 sample possesses the best OER activity among the series of 10%Co_3O_4@n%FeO_x/G-110. The Tafel slope of 10%Co_3O_4@2%FeO_x/G-110 is 63 mV $decade^{-1}$, which is smaller than 80 mV $decade^{-1}$ for 10%Co_3O_4@1%FeO_x/G-110, 76 mV $decade^{-1}$ for 10%Co_3O_4@3%FeO_x/G-110, 78 mV $decade^{-1}$ for 10%Co_3O_4@4%FeO_x/G-110, and 83 mV $decade^{-1}$ for 10%Co_3O_4@5%FeO_x/G-110 (Fig. 5b), revealing an expedited OER kinetics on the 10%Co_3O_4@2%FeO_x/G-110. The results show that high content Fe is not beneficial to the OER due to the poor conductivity of FeO_x. Finally, the effect of crystallization temperature on the OER activity was investigated. As illustrated in Fig. 5c, the optimal hydrothermal treatment temperature should be 110 °C. A higher hydrothermal treatment temperature would lead to further crystallization of FeO_x, which is not favorable to the OER.

The long-term stability of 10%Co_3O_4@2%FeO_x/G-110 was evaluated by chronoamperometry and cyclic voltammetry. As shown in Fig. 6a, the steady-state current densities of 10%Co_3O_4@2%FeO_x/G-110 remain constant even after 25 h, suggesting excellent durability of 10%Co_3O_4@2%FeO_x/G-110 for alkaline OER. After CVs for 2000 cycles, no obvious current attenuation can be observed (Fig. 6b), demonstrating the superior durability of the 10%Co_3O_4@2%FeO_x/G-110 catalyst. After the OER stability test, the sample was analyzed by TEM and XPS. From Fig. S3, the Co_3O_4@FeO_x nanoparticles can be clearly observed on the graphite after the OER test. As displayed in Fig. S4, we can find that the XPS signal of Co 2p is very weak due to lots of water molecules adsorbed on the surface Fe-sites. Moreover, Fe^{2+} and Fe^{3+} ions can be detected in the 10%Co_3O_4@2%FeO_x/G-110 after OER tests. The XPS results suggest that one of the main roles of Fe in the OER should be combined with water molecules, thus accelerating the reaction.

4. Conclusions

In this work, we have demonstrated that core−shell Co_3O_4@-FeO_x showed higher OER activity than the uniformly dispersed $FeCoO_x$ catalyst. The as-synthesized 10%Co_3O_4@2%FeO_x/G-110 shows an overpotential of 318 mV at the current density of 10 mA cm^{-2} and a Tafel slope of 63 mV $decade^{-1}$ in 1 M KOH. Fe plays multiple roles: (1) binding water molecules to promote the OER, (2) improving charge transfer ability of Co_3O_4, and (3) expediting the diffusion of water close to the active sites and oxygen away from the active sites. This research may open up a new route to develop efficient nonprecious metal oxide OER catalysts by supporting iron (oxy)hydroxides onto the surface of other metal oxides.

Data availability

The data that support the findings of this study are available from the corresponding author upon reasonable request.

CRediT authorship contribution statement

N. Liu: Investigation, Data curation. **J. Guan:** Supervision, Conceptualization, Writing − original draft.

Declaration of competing interest

The authors declare that they have no known competing financial interests or personal relationships that could have appeared to influence the work reported in this paper.

Acknowledgments

This work was supported by the National Natural Science Foundation of China (22075099) and the Natural Science Foundation of Jilin Province (20180101291JC).

Appendix A. Supplementary data

Supplementary data to this article can be found online at https://doi.org/10.1016/j.mtener.2021.100715.

References

[1] S. Li, J. Sun, J. Guan, Strategies to improve electrocatalytic and photocatalytic performance of two-dimensional materials for hydrogen evolution reaction, Chin. J. Catal. 42 (2021) 511−556.
[2] Q. Zhang, J. Guan, Single-atom catalysts for electrocatalytic applications, Adv. Funct. Mater. 30 (2020) 2000768.
[3] Y. Li, Y. Sun, Y. Qin, W. Zhang, L. Wang, M. Luo, H. Yang, S. Guo, Recent advances on water-splitting electrocatalysis mediated by noble-metal-based nanostructured materials, Adv. Energy Mater. 10 (2020) 1903120.
[4] H. Sun, Z. Yan, F. Liu, W. Xu, F. Cheng, J. Chen, Self-supported transition-metal-based electrocatalysts for hydrogen and oxygen evolution, Adv. Mater. 32 (2020) 1806326.
[5] F. Lyu, Q. Wang, S.M. Choi, Y. Yin, Noble-metal-free electrocatalysts for oxygen evolution, Small 15 (2019) 1804201.
[6] Q. Zhang, Z. Duan, M. Li, J. Guan, Atomic cobalt catalysts for efficient oxygen evolution reaction, Chem. Commun. 56 (2019) 794−797.

[7] P. Wang, F. Song, R. Amal, Y.H. Ng, X. Hu, Efficient water splitting catalyzed by cobalt phosphide-based nanoneedle arrays supported on carbon cloth, ChemSusChem 9 (2016) 472–477.
[8] W. Chen, H. Wang, Y. Li, Y. Liu, J. Sun, S. Lee, J.-S. Lee, Y. Cui, In situ electrochemical oxidation tuning of transition metal disulfides to oxides for enhanced water oxidation, ACS Cent. Sci. 1 (2015) 244–251.
[9] J.N. Hausmann, S. Mebs, K. Laun, I. Zebger, H. Dau, P.W. Menezes, M. Driess, Understanding the formation of bulk- and surface-active layered (oxy)hydroxides for water oxidation starting from a cobalt selenite precursor, Energy Environ. Sci. 13 (2020) 3607–3619.
[10] L. Liang, H. Cheng, F. Lei, J. Han, S. Gao, C. Wang, Y. Sun, S. Qamar, S. Wei, Y. Xie, Metallic single-unit-cell orthorhombic cobalt diselenide atomic layers: robust water-electrolysis catalysts, Angew. Chem., Int. Ed. 54 (2015) 12004–12008.
[11] J.S. Mondschein, J.F. Callejas, C.G. Read, J.Y.C. Chen, C.F. Holder, C.K. Badding, R.E. Schaak, Crystalline cobalt oxide films for sustained electrocatalytic oxygen evolution under strongly acidic conditions, Chem. Mater. 29 (2017) 950–957.
[12] Y.-C. Liu, J.A. Koza, J.A. Switzer, Conversion of electrodeposited Co(OH)(2) to CoOOH and Co3O4, and comparison of their catalytic activity for the oxygen evolution reaction, Electrochim. Acta 140 (2014) 359–365.
[13] L. Peng, S.S.A. Shah, Z. Wei, Recent developments in metal phosphide and sulfide electrocatalysts for oxygen evolution reaction, Chin. J. Catal. 39 (2018) 1575–1593.
[14] L. Gong, X.Y.E. Chng, Y. Du, S. Xi, B.S. Yeo, Enhanced catalysis of the electrochemical oxygen evolution reaction by iron(III) ions adsorbed on amorphous cobalt oxide, ACS Catal. 8 (2018) 807–814.
[15] S. Wang, T. He, J.H. Yun, Y. Hu, M. Xiao, A. Du, L. Wang, New iron-cobalt oxide catalysts promoting BiVO4 films for photoelectrochemical water splitting, Adv. Funct. Mater. 28 (2018) 1802685.
[16] Y. Lei, R. Huang, H. Xie, D. Zhang, X. Liu, Y. Si, N. Li, Electronic structure tuning of FeCo nanoparticles embedded in multi-dimensional carbon matrix for enhanced bifunctional oxygen electrocatalysis, J. Alloys Compd. 853 (2021) 157070.
[17] F. Pan, Z. Li, Z. Yang, Q. Ma, M. Wang, H. Wang, M. Olszta, G. Wang, Z. Feng, Y. Du, Y. Yang, Porous FeCo glassy alloy as bifunctional support for high-performance Zn-air battery, Adv. Energy Mater. 11 (2021) 2002204.
[18] D. Xie, Y. Chen, D. Yu, S. Han, J. Song, Y. Xie, F. Hu, L. Li, S. Peng, Single-layer carbon-coated FeCo alloy nanoparticles embedded in single-walled carbon nanotubes for high oxygen electrocatalysis, Chem. Commun. 56 (2020) 6842–6845.
[19] Y. Liu, C. Wang, S. Ju, M. Li, A. Yuan, G. Zhu, FeCo-based hybrid MOF derived active species for effective oxygen evolution, Prog. Nat. Sci.: Mater. Int. 30 (2020) 185–191.
[20] M. Tian, Y. Jiang, H. Tong, Y. Xu, L. Xia, MXene-supported FeCo-LDHs as highly efficient catalysts for enhanced electrocatalytic oxygen evolution reaction, ChemNanoMat 6 (2020) 154–159.
[21] N. Trang-Thi Hong, J. Lee, J. Bae, B. Lim, Binary FeCo oxyhydroxide nanosheets as highly efficient bifunctional electrocatalysts for overall water splitting, Chem.-Eur. J. 24 (2018) 4724–4728.
[22] L. Zhuang, L. Ge, Y. Yang, M. Li, Y. Jia, X. Yao, Z. Zhu, Ultrathin iron-cobalt oxide nanosheets with abundant oxygen vacancies for the oxygen evolution reaction, Adv. Mater. 29 (2017) 1606793.
[23] M.S. Burke, M.G. Kast, L. Trotochaud, A.M. Smith, S.W. Boettcher, Cobalt-iron (Oxy)hydroxide oxygen evolution electrocatalysts: the role of structure and composition on activity, stability, and mechanism, J. Am. Chem. Soc. 137 (2015) 3638–3648.
[24] L. Bai, C.-S. Hsu, D. Alexander, H.M. Chen, X. Hu, A cobalt-iron double-atom catalyst for the oxygen evolution reaction, J. Am. Chem. Soc. 141 (2019) 14190–14199.
[25] L. Lv, Z. Yang, K. Chen, C. Wang, Y. Xiong, 2D layered double hydroxides for oxygen evolution reaction: from fundamental design to application, Adv. Energy Mater. 9 (2019) 1803358.
[26] Y. Xia, Y. Xiong, B. Lim, S.E. Skrabalak, Shape-controlled synthesis of metal nanocrystals: simple chemistry meets complex physics? Angew. Chem., Int. Ed. 48 (2009) 60–103.
[27] X. Jia, J. Wu, K. Lu, Y. Li, X. Qiao, J. Kaelin, S. Lu, Y. Cheng, X. Wu, W. Qin, Organic-inorganic hybrids of Fe-Co polyphenolic network wrapped Fe3O4 nanocatalysts for significantly enhanced oxygen evolution, J. Mater. Chem. A 7 (2019) 14302–14308.
[28] H. Jin, S. Mao, G. Zhan, F. Xu, X. Bao, Y. Wang, Fe incorporated alpha-Co(OH)(2) nanosheets with remarkably improved activity towards the oxygen evolution reaction, J. Mater. Chem. A 5 (2017) 1078–1084.
[29] J. Yang, X. Wang, B. Li, L. Ma, L. Shi, Y. Xiong, H. Xu, Novel iron/cobalt-containing polypyrrole hydrogel-derived trifunctional electrocatalyst for self-powered overall water splitting, Adv. Funct. Mater. 27 (2017) 1606497.
[30] Z. Wu, X. Wang, J. Huang, F. Gao, A Co-doped Ni-Fe mixed oxide mesoporous nanosheet array with low overpotential and high stability towards overall water splitting, J. Mater. Chem. A 6 (2018) 167–178.
[31] A.-L. Wang, H. Xu, G.-R. Li, NiCoFe layered triple hydroxides with porous structures as high-performance electrocatalysts for overall water splitting, ACS Energy Lett. 1 (2016) 445–453.
[32] M. Li, L. Bai, S. Wu, X. Wen, J. Guan, Co/CoOx nanoparticles embedded on carbon for efficient catalysis of oxygen evolution and oxygen reduction reactions, ChemSusChem 11 (2018) 1722–1727.
[33] S. Wan, J. Qi, W. Zhang, W. Wang, S. Zhang, K. Liu, H. Zheng, J. Sun, S. Wang, R. Cao, Hierarchical Co(OH)F superstructure built by low-dimensional substructures for electrocatalytic water oxidation, Adv. Mater. 29 (2017) 1700286.
[34] C. Dong, X. Yuan, X. Wang, X. Liu, W. Dong, R. Wang, Y. Duan, F. Huang, Rational design of cobalt-chromium layered double hydroxide as a highly efficient electrocatalyst for water oxidation, J. Mater. Chem. A 4 (2016) 11292–11298.
[35] Q. Zhang, N. Liu, J. Guan, Charge-transfer effects in Fe-Co and Fe-Co-Y oxides for electrocatalytic water oxidation reaction, ACS Appl. Energy Mater. 2 (2019) 8903–8911.
[36] R. Liu, Y. Wang, D. Liu, Y. Zou, S. Wang, Water-plasma-enabled exfoliation of ultrathin layered double hydroxide nanosheets with multivacancies for water oxidation, Adv. Mater. 29 (2017) 1701546.
[37] J.R. Swierk, S. Klaus, L. Trotochaud, A.T. Bell, T.D. Tilley, Electrochemical study of the energetics of the oxygen evolution reaction at nickel iron (Oxy)Hydroxide catalysts, J. Phys. Chem. C 119 (2015) 19022–19029.
[38] C. Wang, J. Zhang, C. Shi, D. Cai, Facile synthesis of Ni-Co LDH nanocages with improved electrocatalytic activity for water oxidation reaction, Int. J. Electrochem. Sci. 12 (2017) 10003–10014.
[39] F. Song, X. Hu, Ultrathin cobalt-manganese layered double hydroxide is an efficient oxygen evolution catalyst, J. Am. Chem. Soc. 136 (2014) 16481–16484.